Field Observations of Sediment Fluxes in the Inner-Surf and Swash Zones

Authors: Butt, Tony, Tinker, Jonathan, Masselink, Gerd, O'Hare, Timothy, and Russell, Paul

Source: Journal of Coastal Research, 2009(254) : 991-1001

Published By: Coastal Education and Research Foundation

URL: https://doi.org/10.2112/08-1044.1

Journal of Coastal Research	25	4	991–1001	West Palm Beach, Florida	July 2009

Field Observations of Sediment Fluxes in the Inner-Surf and Swash Zones

Tony Butt, Jonathan Tinker, Gerd Masselink, Timothy O'Hare, and Paul Russell

School of Earth, Ocean and Environmental Sciences
University of Plymouth
Drake Circus
Plymouth, PL4 8AA, U.K.
tony.butt@yahoo.com
jonathan.tinker@plymouth.ac.uk
gerd.masselink@plymouth.ac.uk
T.OHare@plymouth.ac.uk
P.Russell@plymouth.ac.uk

ABSTRACT

BUTT, T.; TINKER, J.; MASSELINK, G.; O'HARE, T., and RUSSELL, P., 2009. Field observations of sediment fluxes in the inner-surf and swash zones. *Journal of Coastal Research,* 25(4), 991–1001. West Palm Beach (Florida), ISSN 0749-0208.

The behaviour of sediment fluxes is currently less well understood in the inner-surf and swash zones than farther seaward. In the present study, field measurements were obtained of cross-shore velocity and suspended-sediment concentration from 6 and 13 heights above the bed, respectively, between the breakpoint and the shore of an intermediate-to-reflective beach, over a range of hydrodynamic conditions, to examine the cross-shore structure of sediment flux and the physical mechanisms responsible for the observed patterns. Particular attention is given to the inner-surf and swash zones, which are known to contain sediment-transport processes poorly predicted by models based on velocity moments. The cross-shore structure of the depth-integrated, suspended sediment flux is found to vary according to the forcing conditions considerably more in the inner-surf and swash zones than in the outer surf and shoaling zones. In high-energy conditions, fluxes are dominated by a large offshore peak in the outer swash zone, and in low-energy conditions, fluxes are dominated by weak onshore values increasing shorewards. Examination of the temporal and vertical structure of the velocity, sediment concentration, and flux within individual events where offshore transport was dominant reveals that near-bed suspended sediment responds just as readily to mid-water-column velocity shear as to boundary-layer shear. Examination of events in which onshore transport was dominant reveals that near-bed suspended-sediment concentration responds more readily to near-bed horizontal acceleration than to absolute values of near-bed velocity.

ADDITIONAL INDEX WORDS: *Acceleration, hydrodynamics, morphology, shape function, turbulence, velocity shear.*

INTRODUCTION

Morphological change in the nearshore is driven by spatial and temporal gradients of sediment flux. Prediction of sediment flux is still a major challenge, particularly in the inner-surf and swash zones. Models and theories should be tested against field measurements of the sediment flux they are designed to predict, which, in turn, should be as accurate and complete as possible if we are eventually to make predictions of morphological change.

One approach to predicting nearshore evolution is to use parametric models. Rather than attempt to incorporate all the underlying physics, such as with process-based models, these models replace much of the physics with field-based parameterisations of the most important processes. Parametric models of the cross-shore structure of cross-shore sediment flux have recently shown good potential for predicting the medium-term to long-term evolution of beach profiles (*e.g.,* Mariño-Tapia *et al.,* 2007b; Masselink, 2004; Plant, Ruessink, and Wijnberg, 2001; Plant *et al.,* 2004).

Parametric models are often based on the idea of a cross-shore sediment transport *shape function* (the cross-shore distribution of the cross-shore sediment flux across the nearshore). The concept was introduced by Foote, Huntley, and O'Hare (1994), who found a consistent pattern across the nearshore when higher moments of cross-shore velocity were plotted against water depth from a single site. Based on an energetics approach (Bagnold, 1963; Bailard, 1981), higher-order velocity moments could be used as a proxy for sediment flux. It was hypothesised that, as the shape function is advected over the beach with the tide, the characteristic beach profile is developed through cross-shore flux gradients, with divergence and convergence leading to erosion and accretion, respectively. The work was extended by Russell and Huntley (1999), combining data from three different sites. The velocity moments were normalised by the velocity variance, thereby allowing the shape function to be independent of incident wave conditions. A consistent cross-shore flux pattern was found, with chiefly onshore transport in the shoaling zone

DOI: 10.2112/08-1044.1 received 12 March 2008; accepted in revision 28 July 2008.

(predominantly through short-wave skewness) and offshore transport in the surf zone (predominantly through offshore-directed bed return flow). The work was then further extended by Mariño-Tapia *et al.* (2007a), using data from five sites and extending the shape function farther shoreward. The cross-shore distribution of measured sediment fluxes measured at a single height close to the bed was also shown to be consistent with the shape function based on velocity moments, which adds support to the method. The velocity-moments shape function, developed by Mariño-Tapia *et al.* (2007a), was used successfully by Mariño-Tapia *et al.* (2007b) to predict the movement of a breaker bar at Duck, North Carolina, over a 77-day period. An independent test of the shape function concept was performed by Tinker *et al.* (2006), using velocity-moment data from two additional European beaches, and they found excellent correlation with previous results.

However, in the above-mentioned studies, the field instrumentation available at the time, together with the difficulties in making field measurements in high-energy conditions, meant that several important issues were still not able to be fully addressed. Extending the shape function from the breakpoint through to the shoreline, including the swash zone, has been difficult and has only been done tentatively. For example, Weir, Hughes, and Baldock (2006) produced a sediment-flux shape function in the swash zone over a berm, but the sediment fluxes were inferred from morphological measurements, a technique that is inherently limited by the spatial and temporal resolution of the measurements. A swash-zone shape function was produced by Aagaard and Hughes (2006) using measurements of velocity and suspended sediment concentration, but this only extended as far as the seaward limit of the swash zone.

Even though the inner-surf and swash zones have been acknowledged for some time as being very important for nearshore morphological change (*e.g.,* Beach and Sternberg, 1991), the behaviour of the sediment transport in that area is still not as well understood as in areas farther seaward, and the energetics approach has not been able to be applied as successfully (Butt *et al.,* 2005; Hughes, Masselink, and Brander, 1997; Masselink and Hughes, 1998; Puleo and Butt, 2006). The problem was highlighted by Masselink and Russell (2006), who measured in the swash-zone, net offshore-directed higher-order velocity moments but net onshore sediment transport. One reason for this difficulty is the increased importance, in the swash and inner-surf zones, of several physical processes other than the velocity-driven shear stress, upon which the energetics approach is based. These include fluid accelerations (Calantoni and Puleo, 2006; Nielsen, 2002; 2006; Puleo *et al.,* 2003), bore collapse leading to onshore advection of sediment (Jackson, Masselink, and Nordstrom, 2004; Pritchard and Hogg, 2005), large infragravity backwashes advecting sediment offshore (Butt and Russell, 1999; Masselink and Puleo, 2006; Miles, Butt and Russell, 2006), hydraulic jumps (Butt and Russell, 2005), bore turbulence (Butt *et al.,* 2004; Puleo *et al.,* 2000), and in-exfiltration (*e.g.,* Nielsen, 1998; Turner and Masselink, 1998). Velocity shear above the boundary layer through uprush-backwash interaction was also observed by Butt *et al.* (2004) and was suggested as a possible source of turbulence reaching the bed in addition to turbulence originating from the bore.

As the hydrodynamic forcing conditions change, the way in which the combination of these processes influences the cross-shore shape function in the inner surf and swash zones also changes. Therefore, it is important not only to extend the sediment-flux shape function into the inner-surf and swash zones but also to measure the cross-shore distribution of flux under different hydrodynamic forcing conditions. The present study examines the behaviour of the sediment flux and the processes that drive it in the inner-surf and swash zones through field measurements of the cross-shore distribution of sediment flux in that area, under varying offshore conditions.

The present study derives the shape functions from depth-integrated sediment fluxes, calculated using velocity and suspended sediment concentration measurements at several heights above the bed. By using field measurements of fluid velocity and suspended sediment concentration from the inner surf zone to the shoreline, we examine the behaviour of the shoreward part of the sediment flux distribution in high-energy and low-energy conditions. We then investigate the processes that drive these patterns by closely examining instantaneous time series from the inner-swash to the inner-surf zones, together with the vertical and temporal structure of velocity, sediment concentration and flux within individual events.

FIELD EXPERIMENT

The present study forms part of a 3-year international project on cross-shore sediment transport and profile evolution on natural beaches, undertaken between 2004 and 2007. The project involved more instrumentation and data collection than that described in the present article; more general details of which may be found in Tinker *et al.* (2006).

The data used in the present study were collected at Sennen Beach, Cornwall, U.K. (Figure 1), between 8 May 2005 and 26 May 2005. Sennen is a macrotidal (mean spring range $\approx$ 5.3 m) sandy beach (median grain size, $D_{50} \approx 0.57$ mm) that receives a mixture of long-period swell and locally generated windsea, with an annual mean significant wave height of 1.4 m. According to the classification of Masselink and Short (1993), Sennen is a low-tide terrace beach, containing a steeper shoreward section and a more gently sloping seaward section (tan $\beta \approx 0.08$ and 0.03, respectively). During the experiment, morphological surveys were conducted every low tide using a Total Station.

The measurements discussed here were obtained from an instrument rig placed at approximately mean sea level and slightly seaward of the break in slope between the steep shoreward part, and the lower-gradient seaward part of the beach (Figure 2). The movement of the tide caused the swash and surf zones to advect over the rig, causing the relative position of the rig within the surf and swash zones to change with time.

Over the entire experimental period, 36 data-collection runs were performed. Logging was initiated just before the shoreline reached the rig on the incoming tide and was ter-

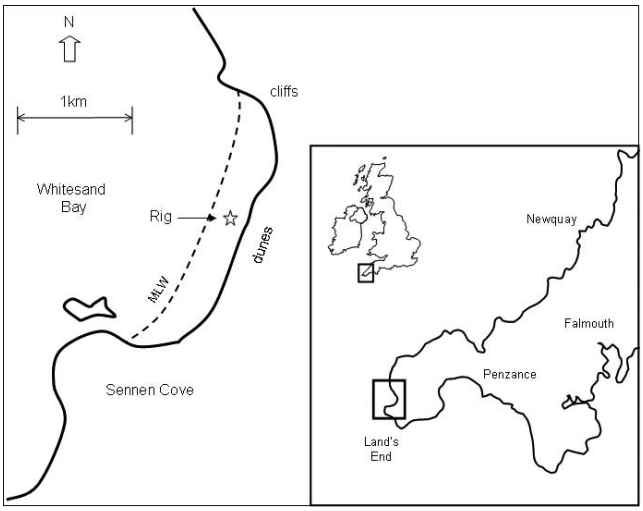

Figure 1. Field site.

minated just after the shoreline receded past the rig on the outgoing tide. Each run was approximately 6 to 7 hours long. Offshore significant wave heights and peak spectral periods were recorded by an acoustic Doppler current profiler (ADCP), deployed on the bed approximately 600 m offshore in 16 m of water.

The instrumentation used to collect the data for the present study (Figure 3) consisted of the following:

- A vertical stack of six Valeport miniature electromagnetic current meters (ECMs) measuring cross-shore (u) and alongshore (v) components of velocity at distances above the bed (z) of 3, 6, 9, 13, 19, and 29 cm;
- A Druck miniature pressure transducer (PT), measuring water depth (h), nominally mounted 2 cm below the sand surface, with the position of the instrument relative to the bed carefully measured before and after each data collection run; and
- A vertical array of 13 miniature optical backscatter sensors, measuring suspended sediment concentration (c) at $z = -2, -1, 0, 1, 2, 3, 4, 5, 6, 9, 13, 19, 29$ cm, with sensors similar to those described in Masselink and Russell (2006), developed in-house at the University of Plymouth, and calibrated using the method developed by Butt *et al.* (2002).

All instruments were logged synchronously at 8 Hz using a National Instruments data logger mounted on the rig itself. The digitized signal was routed to a logging computer at the top of the beach *via* an RS485 data link. Power for the rig was supplied by cable from the logging station.

A cross-shore profile of measurements was able to be obtained from a fixed instrument rig, by allowing the tide to flood or ebb over the rig. The reference frame may, thence, be transferred from time to distance or, in this case, to normalised depth (= local depth over breaker depth, h/h_b). In the present study, the approximate position of the breakpoint was estimated using a fixed ratio of breaker height to breaker depth ($H_b/h_b = 0.78$; McCowen, 1894), although it is acknowledged that, in a random wave field, the breakpoint varies considerably either side of this value.

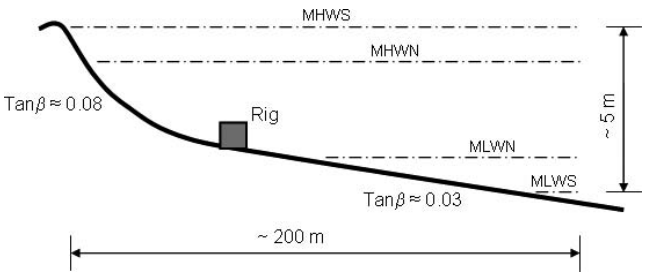

Figure 2. Beach profile showing rig position. MHWS = mean high-water springs; MHWN = mean high-water neaps; MLWN = mean low-water neaps; and MLWS = mean low-water springs.

DATA PREPROCESSING

The raw data were screened as follows. The suspended-sediment data were rejected if they showed any signs of contamination by daylight. Sections of data in which there was a dropout in the velocity from the lowest ECMs, because of the instrument being buried, were also rejected, along with data in which the bed level had dropped below the level of the PT. Noisy data because of the instruments being very near the surface were also rejected by using the water depth (h) time series to ensure that velocity and suspended sediment data were only considered for analysis when the instruments were covered by 0.5 cm of water.

The breaking wave height (H_b) and breaker depth (h_b) were estimated from the data collected at the ADCP. Using linear wave theory it may be shown that

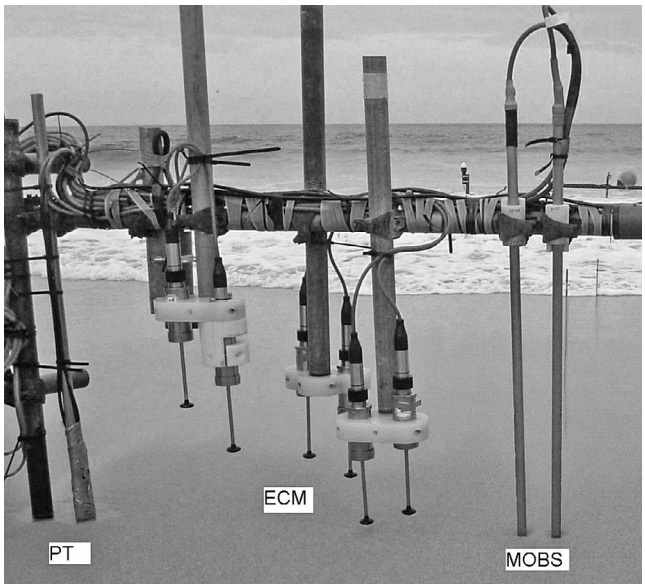

Figure 3. Instrument rig.

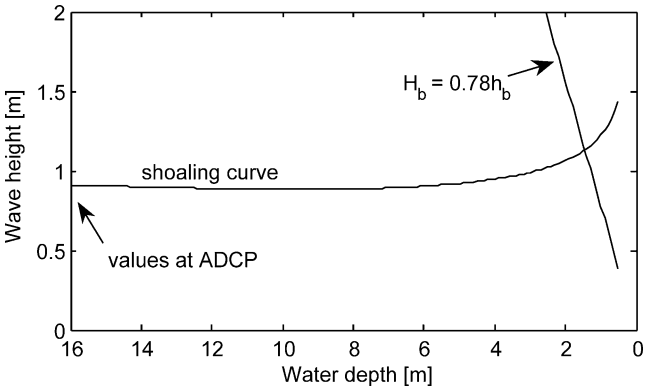

Figure 4. Example plot showing how values of H_b and h_b were estimated. Initial values of wave height and water depth were obtained from the ADCP.

$$H_2 = H_1\sqrt{\frac{C_{g2}}{C_{g1}}} \tag{1}$$

where H is the wave height, and C_g is the group velocity, which is a function of the water depth (h) and the wavelength (L), which, in turn, may be estimated from the period (T). The waves were shoaled in to obtain H as a function of h, using initial values of H, T, and h (= 16 m) at the ADCP. The points at which $h = h_b$ and $H = H_b$ were then found using $H_b/h_b = 0.78$. An example is shown in Figure 4.

The resultant time series of H_b throughout the experiment is shown in Figure 5. A distinct change from relatively low to relatively high energy conditions can be seen around the 18th of May.

To validate sediment-transport predictions, the measured suspended-sediment flux is usually calculated from the product of the velocity and suspended-sediment concentration, measured using colocated instruments. Although vertical stacks of optical backscatter sensors have been used for some time (*e.g.,* Beach, Sternberg, and Johnson, 1992) most surf-zone and swash-zone sediment transport field studies, apart from a small number of exceptions (*e.g.,* Miller, 1999), have tended to deploy current meters at three or less locations in the vertical. It has often been assumed that the velocity is depth-uniform above the boundary layer, and discussions on whether the velocity measured at a single height can safely be assumed depth-uniform have been based on the thickness of the boundary layer (*e.g.,* Petti and Longo, 2001). However, more recent observations (*e.g.,* Butt *et al.,* 2004) have suggested that, in the swash zone, there is considerable velocity shear above the boundary layer, which varies throughout the wave cycle. Therefore, to obtain more accurate estimates of depth-integrated flux, it is important to measure both suspended sediment and velocity at as many positions in the vertical as possible. In the present study, vertical stacks of six current meters and 13 optical backscatter sensors, throughout the lower 29 cm of the water column were used to calculate the depth-integrated sediment flux. It is acknowledged that, particularly in the swash zone, a proportion of the sediment transport occurs as bedload (*e.g.,* Horn and Mason, 1994), which would not be measured by the instrument arrangement described here.

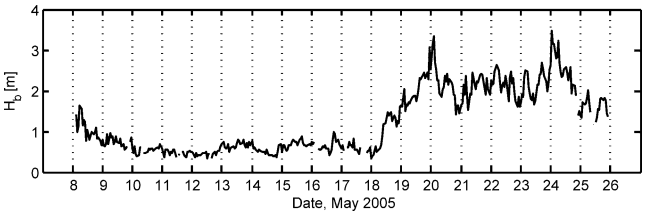

Figure 5. Time series of breaking wave height throughout the experiment. Dates on the x-axis correspond to 1200 on each particular day.

The depth-integrated suspended-sediment flux (Q) was calculated by multiplying the velocity and the suspended-sediment concentration at each individual height, and then integrating throughout the water column, *i.e.,*

$$Q = \int u(z)c(z)\,dz. \tag{2}$$

In practice this was achieved by summing over the water column the products of u, C, and the thickness of the "slice" (Δz) at each height measured, *i.e.,*

$$Q = u_1c_1\Delta z_1 + u_2c_2\Delta z_2 + \cdots + u_nc_n\Delta z_n. \tag{3}$$

For the uppermost sensor, the thickness of the slice was taken as the average of the distance between the sensor and its lower neighbour and a point 10 cm above the sensor. Inspection of the data revealed that very little measurable flux was present at the top sensor; therefore, it was assumed that the concentration above this layer was zero. For the intermediate sensors, the thickness of the slice was the average of the distance between the sensor and its upper and lower neighbour, respectively. For the lowest sensor, it was the average of the distance between the sensor and its upper neighbour and the distance between the sensor and the bed.

The depth-integrated suspended-sediment concentration (C) was calculated in the same way as the depth-integrated flux, *i.e.,*

$$C = \int c(z)\,dz, \tag{4}$$

i.e.,

$$C = c_1\Delta z_1 + c_2\Delta z_2 + \cdots + c_n\Delta z_n. \tag{5}$$

FLUX RESPONSE TO HYDRODYNAMIC CONDITIONS

To examine the hypothesis that the sediment flux, as a function of cross-shore distance, changes according to the forcing conditions, it was considered instructive to inspect the cross-shore distribution of the depth-averaged suspended-sediment flux under low- and high-energy conditions, focusing on the surf and swash zones.

Five-minute averages of the depth-integrated flux, $\langle Q \rangle$, were computed for four high-energy and five low-energy runs.

Table 1. *Low-energy runs. Suffix* a *or* b *indicates data used from the rising or falling tide, respectively. The value of* H_b *for run 06 was estimated visually.*

Run	06*a*	08*a*	23*a*	23*b*	25*b*
Date, May 2005	8	9	16	16	17
H_b (m)	0.6	0.7	0.6	0.6	0.6
σ_u (m^2 s^{-2})	0.16	0.10	0.08	0.08	0.05

Table 2. *High-energy runs. Suffix* a *or* b *indicates data used from the rising or falling tide, respectively.*

Run	29*a*	31*a*	33*a*	35*a*
Date, May 2005	19	20	22	23
H_b (m)	1.7	1.9	1.8	1.9
σ_u (m^2 s^{-2})	0.22	0.19	0.23	0.22

For the purposes of this test, a run was considered to be *high energy* if $H_b > 1$ m and *low energy* if $H_b < 1$ m. Tables 1 and 2 show values of H_b and near-bed cross-shore velocity variance (σ_u) of the runs used for analysis.

Figure 6 shows $\langle Q \rangle$ as a function of normalised depth, h/h_b. The 5-minute average value of h-h_b can be used as a rough proxy for normalised distance between the shore and the breakpoint, which allows direct comparison between more than one time series. In the swash zone, during times when the instruments were not inundated, the depth was classed as zero. Therefore, even though in the swash zone the instantaneous depth is related to the shape of the swash lens rather than the cross-shore position, the average depth will decrease towards the shore as the inundation time decreases.

Note that an alternative method for estimating the cross-shore position in the swash zone is to directly measure the relative percentage of time that the bed is inundated, which is zero at the shoreline and increases seaward until the outer limit of the swash zone where it is 100% (*e.g.,* Aagaard and Hughes, 2006; Hughes and Moseley, 2007; Masselink and Russell, 2006). However, the method used was considered adequate for the purposes of the present study rather than combining two different techniques for the swash and surf zones.

The data from all the high-energy runs were grouped separately from those of the low-energy runs. The values of $\langle Q \rangle$ were then separated into bins of width $\Delta(h/h_b) = 0.1$ (high energy) and $\Delta(h/h_b) = 0.2$ (low energy), and the mean value of $\langle Q \rangle$ over each bin was calculated. The minimum number of points in each bin was 10. The error bars on the bin averages represent ± 2 standard errors. The spline fit through the bin averages is simply to visualise the cross-shore distribution of sediment flux. An estimate of the outer limit of the swash zone was obtained by inspecting the instantaneous depth (h) time series and identifying two successive 5-minute blocks of data whereby the bed was intermittently wet and dry during the shoreward block and continually wet during the seaward block. The outer limit of the swash zone was then assumed to lie midway between these two blocks. Note that, in practice, the outer edge of the swash zone can never be a single, well-defined cross-shore position. However, the simple definition described here is considered adequate for the analysis in the present study. For more rigorous definitions, see Hughes and Moseley (2007).

Figure 6 shows how the behaviour of the cross-shore flux distribution in the inner-surf and swash zones differs under high-energy and low-energy conditions. In both cases, the magnitude of the depth-integrated flux begins to increase landward from around the inner surf zone. The low-energy data show a weak onshore flux progressively increasing towards the shore. Offshore of the inner surf zone, the low-energy data show a very weak, almost zero, flux. The high-energy flux contains a large offshore-directed peak in the mid to outer swash zone, which is about an order of magnitude larger than the maximum onshore flux shown on the low-energy plot. Offshore of the inner surf zone, the high-energy data show a relatively weak general offshore flux.

To visualise how the behaviour of the cross-shore sediment flux might act on the same section of beach face, both sets of $\langle Q \rangle$ values were plotted on the same axes, as a function of cross-shore distance, x. Values of x, corresponding to each value of $\langle Q \rangle$, were found using $x = h/\tan\beta$, assuming x increases seawards and $x = 0$ when the rig is at the shoreline. Results (Figure 7) broadly show the same pattern of strong offshore transport in high-energy conditions and weak onshore transport close to the shore in low-energy conditions.

It must be stressed that the *tidal advection* technique, as used in the present study, suffers from the limitation that, because the cross-shore position was inferred from the depth of water over a fixed section of bed, any implications for morphological change derived from the flux gradients are only applicable on sections of the profile with the same slope as that at the instrument site. For example, they would not be directly applicable to the beach in the present study at the high-tide shoreline, where the slope was significantly differ-

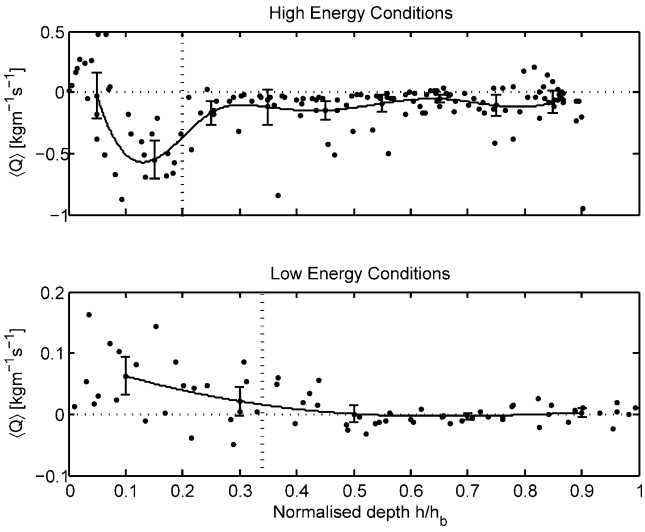

Figure 6. Cross-shore distribution of suspended-sediment flux for high-energy and low-energy conditions. The vertical dotted line is the approximate outer limit of the swash zone. Points with error bars are bin averages, explained in the text. The solid line is a spline fit. Note difference in y-axis scaling.

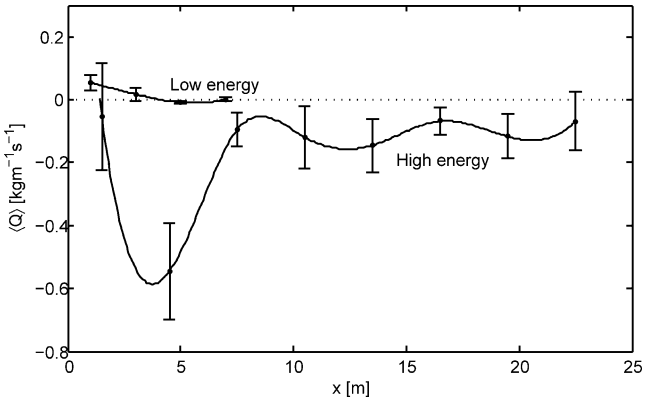

Figure 7. Sediment flux as a function of cross-shore distance, for low-energy and high-energy conditions. The original values of $\langle Q \rangle$ have been removed for clarity. Each function extends from the shoreline to the approximate breakpoint.

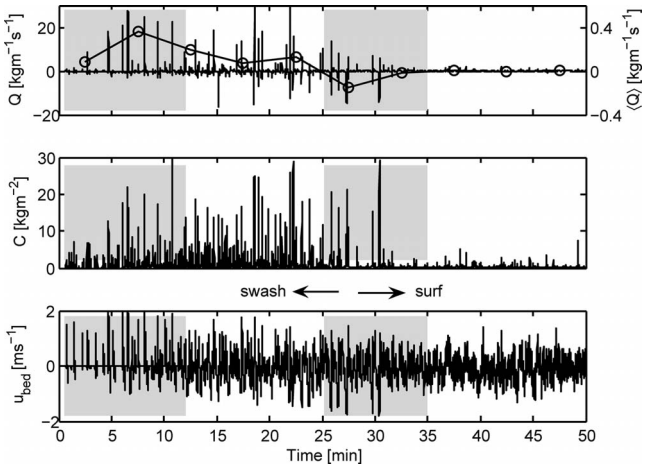

Figure 8. Time series showing where large sediment-suspension events start. The line with circles in the upper panel shows $\langle Q \rangle$. The grey areas correspond to the inner and outer expanded time series in Figures 9 and 10.

ent. Here, the input conditions to the section of bed being considered would be very different from those at the rig.

INSTANTANEOUS TIME SERIES

It was considered instructive to inspect more closely the instantaneous sediment-flux time series to investigate the processes that contribute to onshore and offshore transport at different points in the cross-shore transect, focusing particularly on the inner-surf and swash zones. The data chosen for examination here are from a medium-energy run (run 04; 7 May 2005), where the value of H_b ($\approx$1 m, estimated visually) was at the transition between the high-energy and low-energy data used in the tests above (and, therefore, were not used in those tests). The purpose of using this run is that it serves as a good example where the behaviour of the cross-shore sediment flux includes features seen in both high-energy and low-energy conditions. In the following analysis, particular sections of data where either onshore or offshore transport dominates are examined.

Figure 8 shows, as a function of time, instantaneous values of depth-integrated flux (Q), suspended sediment concentration (C) and near-bed velocity measured at $z = 3$ cm (u_{bed}), from when the instrument rig was at the shoreline to when $h/h_b \approx 0.65$. Five-minute flux averages ($\langle Q \rangle$) are also shown for comparison. At around $t \approx 30$ minutes (*i.e.,* just beyond the swash outer limit), large values of suspended sediment begin to appear. These coincide with the onset of large backwashes, manifest as offshore-directed peaks in the velocity time series. As the shoreline is approached, the velocity time series becomes progressively more dominated by onshore values. In the flux time series, offshore events practically disappear. It is important to realise that the resulting flux is highly sensitive to the phase between the velocity and the sediment concentration (Osborne and Rooker, 1999). In Figure 8, the flux becomes more onshore directed as the observer approaches the shore, not just because the velocity time series contains progressively more onshore-dominated and progressively less offshore-dominated events, but also because the peaks in C coincide with onshore rather than offshore peaks in u_{bed}.

A 10-minute segment of the time series in Figure 8, representing the part where offshore sediment flux events begin (around the surf/swash transition zone; $t = 25$ to 35 mins) is shown expanded in Figure 9. The large values of suspended sediment appear between the end of the offshore phase and the beginning of the next onshore phase of each event. This has been observed several times in previous studies (*e.g.,* Butt and Russell, 1999; Osborne and Rooker, 1999; Puleo *et al.,* 2000). Large increases in C only seem to occur in the backwashes, where the offshore velocity exceeds about 1 m s^{-1}. For the five large backwashes in Figure 9, (at $t \approx 25.9$, 26.5,

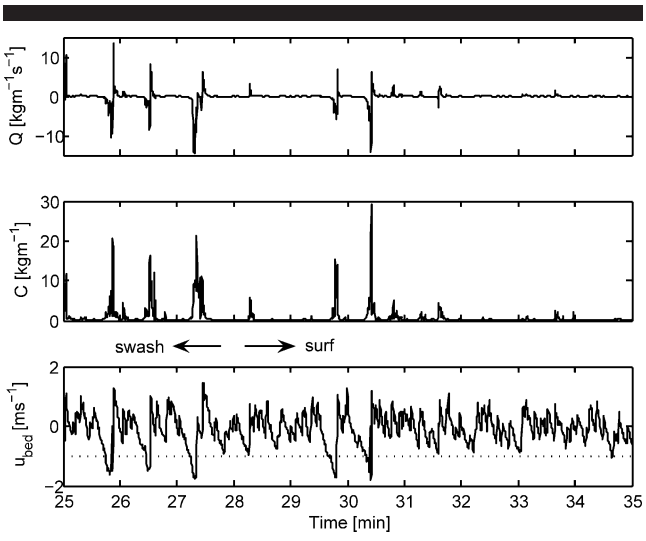

Figure 9. Swash/surf transition zone instantaneous time series. The dotted line in the lower panel represents an arbitrary velocity threshold, above which, large suspension events seem to occur.

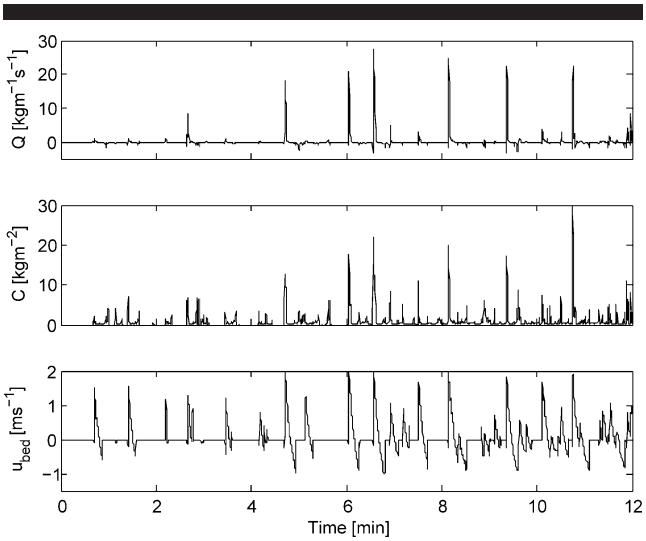

Figure 10. Inner to mid-swash instantaneous time series.

27.3, 29.8, and 30.4 mins), the value of C begins to increase only after the velocity has reached that value. For the remaining backwashes in the time series, C is much smaller or insignificant.

Figure 10 shows a 12-minute segment of the time series from the inner swash to the mid swash zone. Here, it can be seen that the major sediment-suspension events only occur in conjunction with onshore velocities. The six distinct onshore flux events (at $t \approx 4.7$, 6.0, 6.6, 8.2, 9.4, and 10.8 mins) occur during events containing the highest onshore velocities.

STRUCTURE OF INDIVIDUAL EVENTS

To further investigate the way in which sediment is transported within individual waves between the inner surf zone and the shoreline, the cross-shore velocity (u), suspended sediment concentration (c), and flux (q), as a function of both time and vertical distance from the bed, were more closely examined for typical offshore-transporting and onshore-transporting events, such as those in Figures 9 and 10, from the outer-swash/inner-surf and from the mid to inner swash, respectively.

Ensemble averages of *u, c,* and *q,* together with the depth-integrated flux (Q) velocity shear (du/dz) and cross-shore acceleration (du/dt), were computed using seven offshore-transporting events from the outer-swash/inner-surf zone. This was repeated using nine onshore-transporting events from the mid to inner swash zone. Events were chosen to have a clear start and end, and peak values of u exceeding 1 m s^{-1}. The length of each event was taken as 5 second either side of the time of occurrence of the local minimum depth in the case of offshore events and 2 second before and 5 second after the local minimum depth in the case of onshore events. Because all members of the ensemble average were the same length, there was no need to stretch them by interpolation, as is often done with ensemble averages using field data (*e.g.,* Masselink *et al.,* 2005). To qualify as an offshore or onshore event, the total sediment discharge (the depth-integrated, time-integrated flux over that event) in that direction had to be at least 1.5 times the total sediment discharge in the other direction.

Ensemble-averaged offshore (outer) and onshore (inner) events are shown in Figures 11 and 12, respectively. For comparison, Q, q, c, and u for representative single events are shown next to the ensemble averages. The similarity of these plots to the ensemble averages adds confidence to the ensemble averages. To obtain a rough indication of the spread in values over the ensemble averages, mean ensemble-averaged values of *u, c* and *q,* alongside their corresponding mean values of standard error, are shown in Table 3. The peak velocities are also shown for comparison to give an indication of the strength of the wave stirring. Interestingly, the mean value of q (11.8 kg m^{-2} s^{-1}) for the inner event is much higher than that for the outer event (-3.6 kg m^{-2} s^{-1}), although the mean values of u and c for both events are similar.

From the ensemble-averaged event in Figure 11, the following observations can be made. The near-bed velocity is strongly offshore during the backwash but continues offshore until about 1.5 seconds after the arrival of the bore (indicated by a sharp increase in water depth) at the measuring point. The velocity higher in the water column increases onshore after the arrival of the bore, reaching a local maximum after about 1.2 seconds. There is considerable velocity shear between $z \approx 8$ cm and $z \approx 12$ cm, just after the arrival of the bore, which is about four times stronger than the shear in the boundary layer. For about 1 second, there is actually velocity reversal in the water column (offshore near the bed but onshore at higher levels). It can be seen by simply comparing c with u that high values of c occur where the two opposing flows meet and the offshore flow undercuts the onshore flow. This is the point at which there is the largest general velocity gradient (*i.e.,* the contours are closest together). Peak near-bed c values can be seen about 0.6 seconds after peak values of du/dz higher in the water column. There appears to be little direct relationship between c and du/dt. The large offshore values of Q at $t \approx 1$ second are due to high values of c and offshore u near the bed, whereas the onshore peak in Q at $t \approx 1.5$ second is due to weaker values of c and onshore u spread over a thicker layer of water, higher in the water column.

From the ensemble-averaged event in Figure 12, the following observations can be made. The velocity is weakly offshore near the bed until about 0.5 second after the arrival of the bore; after which, it increases onshore at all heights in the water column, reaching a peak after about 1.5 second. There is no velocity reversal in the water column. There is a degree of shear in the mid water column, but the boundary-layer shear is about twice as strong. The onshore flow is much more dominant than in the offshore event, and is not undercut by the (much weaker) offshore flow. Peak c values, as with the offshore event, coincide with the largest general velocity gradient (where the contours are closest together). The contours are mostly vertical suggesting a stronger horizontal than vertical velocity gradient. Peak near-bed c values occur about the same time as, or just after, large near-bed du/dt values, but they occur about 0.3 second before peak u

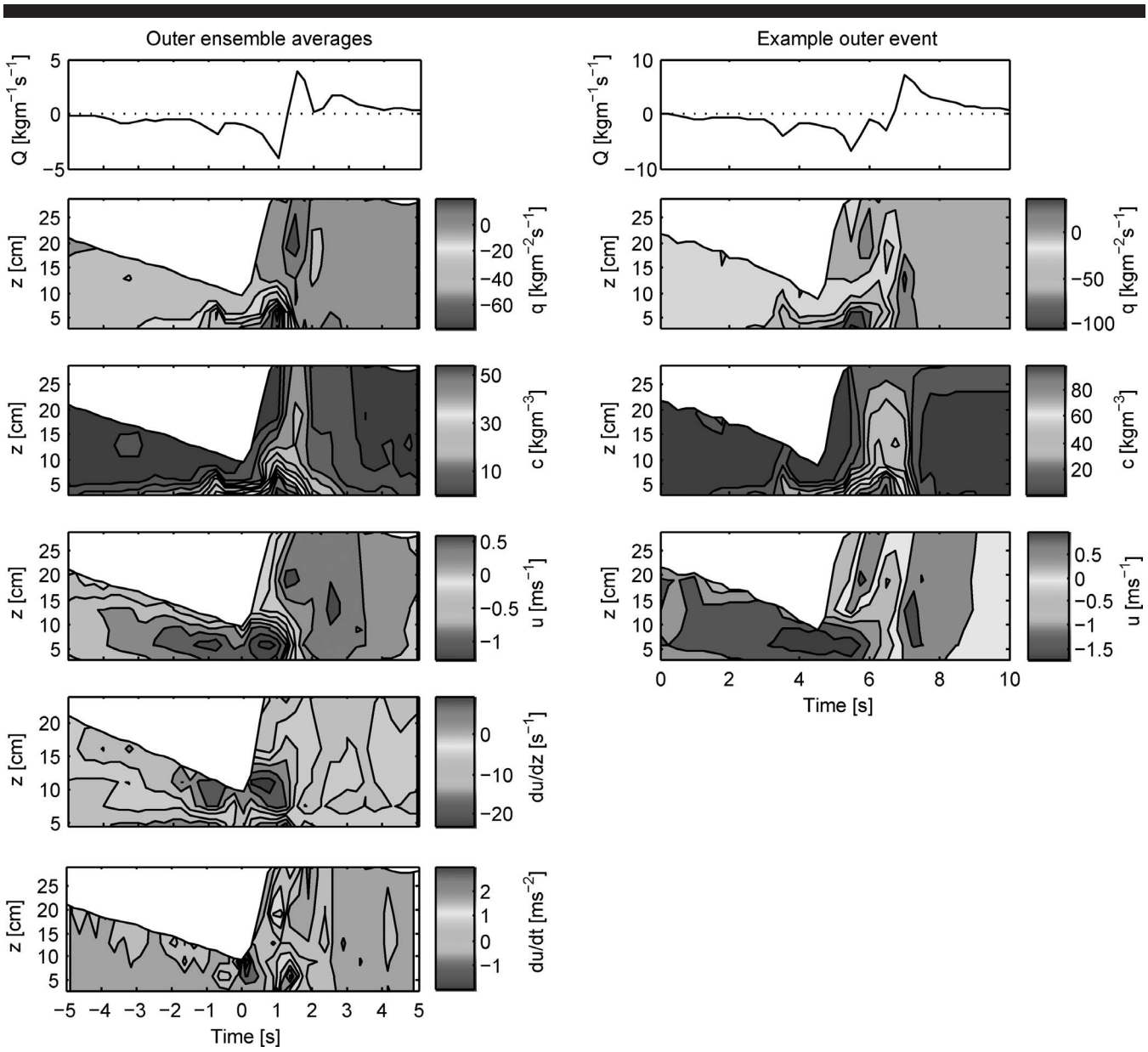

Figure 11. Ensemble-averaged (left panels) and example (right panels) events from outer-swash/inner-surf zone. On the ensemble average, time = 0 corresponds to the local minimum depth. **For a color version of this figure, see page 932.**

values. The fact that maximum acceleration leads maximum velocity supports the idea that suspended sediment is responding to acceleration. There appears to be little direct relationship between c and du/dz.

DISCUSSION

Figures 6 and 7 show that the cross-shore distribution of suspended-sediment flux in the inner-surf and swash zones is clearly not the same in high-energy conditions (defined as $H_b > 1$ m) as in low-energy conditions (defined as $H_b < 1$ m). The most significant differences in high-energy and low-energy conditions are in the swash zone.

The contour plots in Figures 11 and 12 highlight the complexity of the vertical structure of the fluid and sediment in the swash and inner surf zones and suggest that different combinations of several mechanisms acting on the bed to suspend sediment may exist at different times during the wave cycle. The relative temporal phase between the peaks in velocity and suspended sediment concentration supports the idea that, in the swash zone, sediment suspension may be produced by mechanisms other than near-bed velocity shear. If near-bed velocity shear were the dominant mechanism, the peaks would be expected to be in phase (or at least with a constant phase shift associated with the time taken for sed-

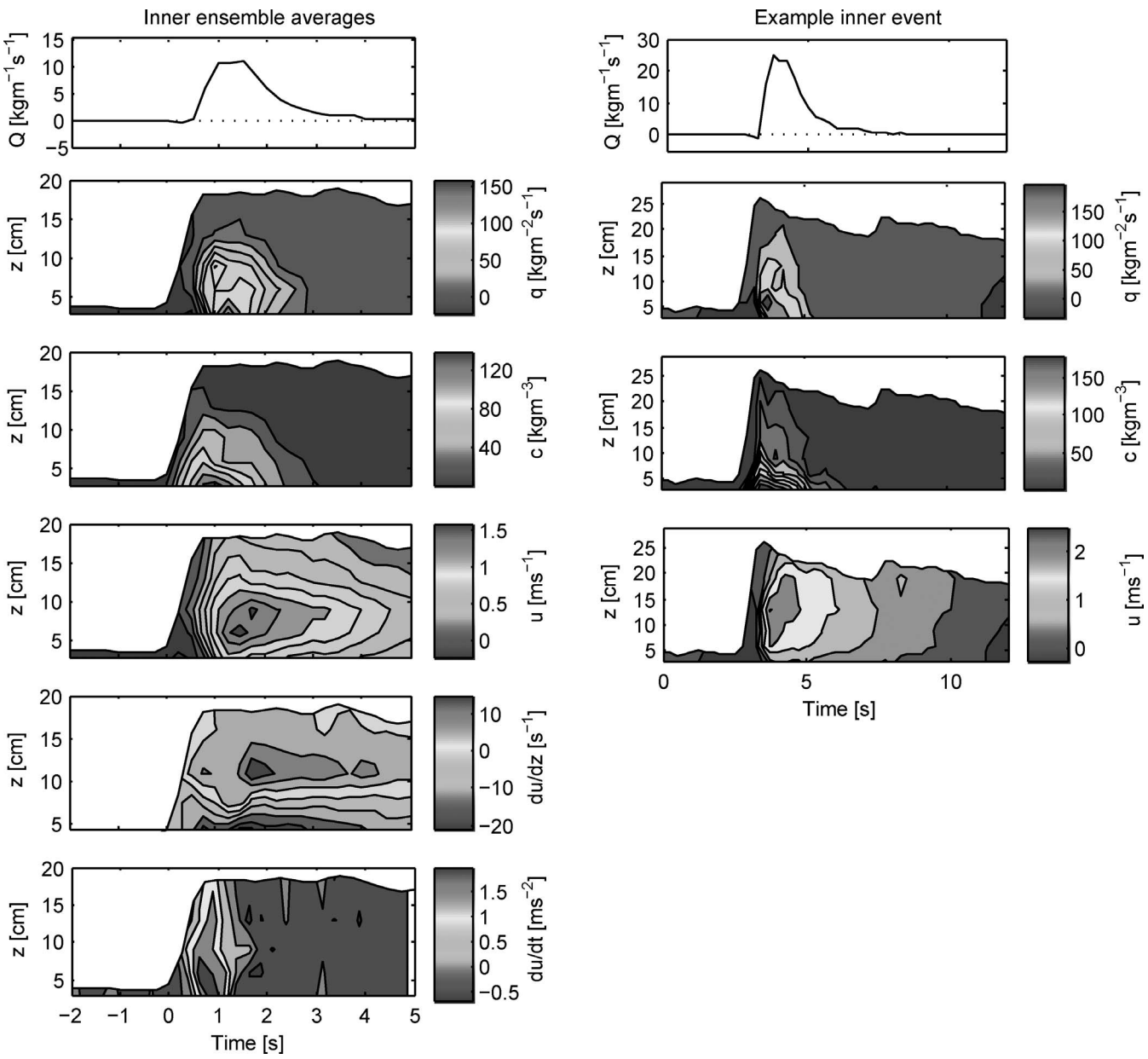

Figure 12. Ensemble-averaged (left panels) and example (right panels) events from mid to inner swash zone. On the ensemble average, time = 0 corresponds to the local minimum depth. **For a color version of this figure, see page 933.**

Table 3. *Mean ensemble-averaged values and mean standard error.*

	Offshore (N = 7)			Onshore (N = 9)		
Metric	u (m s^{-1})	c (kg m^{-3})	q (kg m^{-2} s^{-1})	u (m s^{-1})	c (kg m^{-3})	q (kg m^{-2} s^{-1})
Mean	−0.24	8.4	−3.6	0.17	8.9	11.8
Mean standard error	0.12	3.5	3.5	0.06	2.9	4.7
Peak velocity	−1.24			1.68		

iment to travel upwards from the bed to a measurement height). However, the peaks would not necessarily be in phase if other mechanisms, such as bore turbulence (*e.g.,* Butt *et al.,* 2004; Puleo *et al.,* 2000), acceleration (*e.g.,* Calantoni and Puleo, 2006; Nielsen, 2002; 2006; Puleo *et al.,* 2003), or in-exfiltration (*e.g.,* Nielsen, 1998; Turner and Masselink, 1998), were significantly contributing to the sediment suspension. The fact that the near-bed peak in suspended sediment concentration occurs about 0.6 s after the peak in the mid-water-column velocity shear suggests a possible link between sediment suspension and turbulence caused by uprush-backwash interaction. During the arrival of the bore at the measurement position, Butt *et al.* (2004) measured increasing water depths at the same time as increasing offshore velocities near the bed. This suggested the possibility of mid-water-column velocity shear whereby the bore would be forcing the flow onshore in the upper water column, while the backwash flow still dominated in the lower water column. Those observations, which were made using measurements from a single height, are supported by the vertical profile of measurements from the present study.

The fact that there were no vertical (w) velocity measurements in the present study precludes analysis of the vertical structure of the velocity including all three components, or turbulence analysis in terms of Reynolds stresses, both of which might reveal information on sediment-suspension mechanisms. For example, Aagaard and Hughes, (2006) observed strong vertical velocity fluctuations in the swash zone at the leading edge of the uprush and discuss several possible mechanisms that might be producing them, including turbulent eddies advected shoreward from the inner surf zone and the phenomenon of downbursting, as previously observed in the laboratory by Kubo and Sunamura (2001). Therefore, further work to the present study might include examining the structure of all three velocity components within individual events.

Presuspended sediment being advected shorewards by flows higher in the water column than those upon which velocity-moment calculations are based would also affect the overall direction and magnitude of the transport, particularly in the outer-swash and inner-surf zones. This can be seen in Figure 11, where relatively weak onshore fluxes between $z \approx 10$ cm and $z \approx 29$ cm result in depth-integrated fluxes of a similar magnitude to the offshore depth-integrated fluxes produced by much stronger fluxes confined close to the bed. The velocity shear in Figure 11 shows that the near-bed velocity remains offshore for a considerable time after the arrival of the bore (indicated by a sharp rise in depth), even when the velocity higher in the water column is already onshore (*e.g.,* Butt *et al.,* 2004). Very little work has been done on advection of presuspended sediment in the swash zone, apart from that associated with bore collapse (Jackson, Masselink, and Nordstrom, 2004; Pritchard and Hogg, 2005).

The ensemble-averaged event from the inner swash zone (Figure 12) shows a possible relationship between suspended-sediment concentration and acceleration ($t \approx 0.9$ s). Acceleration has been suggested in previous studies (*e.g.,* Nielsen *et al.,* 2002; 2006; Puleo *et al.,* 2003) to be important for sediment suspension, although it is still not clearly understood whether, in the inner-surf and swash zone, the dominant mechanism may be bore turbulence because high accelerations have been generally measured when turbulent vortices from the bore are likely to be reaching the bed. For example, Puleo *et al.* (2003) suggest that the inclusion of an acceleration term in a simple sediment-transport model improves the model because it encompasses bore turbulence as well as horizontal pressure gradients associated with the accelerating portion of the uprush.

CONCLUSIONS

The cross-shore distribution of suspended-sediment flux, with particular emphasis on the inner-surf and swash zones, has been derived from field measurements in different hydrodynamic forcing conditions. Using measured fluxes, rather than inferring the fluxes from velocity moments, is essential because of the existence of non-energetics type sediment-transport processes in the inner-surf and swash zones.

The flux distribution is clearly not the same in high-energy conditions as it is in low-energy conditions in the inner-surf and swash zones, but it is similar in the outer-surf and shoaling zones. In high-energy conditions, the flux distribution is dominated by a large offshore-directed peak in the outer swash zone, and in low-energy conditions, the dominant feature is a weak, onshore-directed flux in the swash zone, increasing towards the shore.

The processes that drive the above patterns have been more closely investigated by examining instantaneous time series together with the vertical and temporal structure of velocity, sediment concentration, and flux within individual events.

In individual events, where offshore transport was dominant (typical of the outer-swash and inner-surf zones in high-energy conditions), the vertical structure suggests that suspended sediment responds just as readily to mid-water-column velocity shear from the uprush-backwash interaction as to boundary-layer shear, suggesting that the former could be significant for sediment transport.

In individual events, where onshore transport was dominant (typical of the mid-to-inner swash zone in low-energy conditions), the vertical structure is quite different and suggests that the suspended sediment responds more readily to near-bed fluid acceleration than to near-bed velocity.

ACKNOWLEDGMENTS

We would especially like to thank Peter Ganderton for providing expert technical support for the field experiment. Further field assistance was provided by various members from the Coastal Processes Research Group at the University of Plymouth. We are also grateful to the King family for allowing us to temporarily convert their holiday home into a field laboratory. This research was funded by a NERC grant (NER/A/S/2003/00553) "Cross-shore sediment transport and profile evolution on natural beaches (X-Shore project)."

LITERATURE CITED

Aagaard, T. and Hughes, M., 2006. Sediment suspension and turbulence in the swash zone of dissipative beaches. *Marine Geology,* 228, 117–135.

Bagnold, R.A., 1963. Mechanics of marine sedimentation. *In:* Hill, M.N. (ed.), *The Sea,* Volume 3, New York: Wiley Interscience, pp. 507–528.
Bailard, J.A., 1981. An energetics total load sediment transport model for a plane sloping beach. *Journal of Geophysical Research,* 86, 10938–10954.
Beach, R.A. and Sternberg, R., 1991. Infragravity-driven suspended sediment transport in the swash, inner and outer surf zone. *In: Proceedings of Coastal Sediments, '91.* (Seattle, Washington, ASCE), pp. 114–128.
Beach, R.A.; Sternberg, R., and Johnson, R., 1992. A fiber optic sensor for monitoring suspended sediment. *Marine Geology,* 103, 513–520.
Butt, T. and Russell, P., 1999. Suspended sediment transport mechanisms in high-energy swash. *Marine Geology,* 161, 361–375.
Butt, T.; Miles, J.: Ganderton, P., and Russell, P., 2002. A simple method for calibrating optical backscatter sensors in high concentrations of non-cohesive sediments. *Marine Geology,* 192, 419–424.
Butt, T. and Russell, P., 2005. Observations of hydraulic jumps in high energy swash. *Journal of Coastal Research,* 21, 1219–1227.
Butt, T.; Russell, P.; Puleo, J., and Masselink, G. 2005. The application of Bagnold-type sediment transport models in the swash zone. *Journal of Coastal Research,* 21, 887–895.
Butt, T.; Russell, P.; Puleo, J.; Miles, J., and Masselink, G., 2004. The influence of bore turbulence in the swash and inner surf zones. *Continental Shelf Research,* 24, 757–771.
Calantoni, J. and Puleo, J., 2006. Role of pressure gradients in sheet flow of coarse sediments under sawtooth waves. *Journal of Geophysical Research,* 111, C01010, doi: 10.1029/2005JC002875.
Foote, Y.; Huntley, D., and O'Hare, T., 1994. Sand transport on macrotidal beaches. *In: Proceedings of the Euromech 310 Colloquium,* Le Havre, France: World Scientific, pp. 360–374.
Horn, D. and Mason, T. 1994. Swash zone sediment transport modes. *Marine Geology,* 120, 309–325.
Hughes, M. and Moseley, A. 2007. Hydrokinematic regions within the swash zone. *Continental Shelf Research,* 27, 2000–2013.
Hughes, M.; Masselink, G., and Brander, R. 1997. Flow velocity and sediment transport in the swash zone of a steep beach. *Marine Geology,* 138, 91–103.
Jackson, N.; Masselink, G., and Nordstrom, K., 2004. The role of bore collapse and local shear stresses on the spatial distribution of sediment load in the uprush of an intermediate-state beach. *Marine Geology,* 203, 109–118.
Kubo, H. and Sunamura, T., 2001. Large-scale turbulence to facilitate sediment motion under spilling breakers. *In: Proceedings of Coastal Dynamics '01.* (Lund, Sweden, ASCE), pp. 212–221.
Mariño-Tapia, I.; Russell, P.; O'Hare, T.; Davidson, M., and Huntley, D., 2007a. Cross-shore sediment transport on natural beaches and its relation to sand bar migration patterns, part 1: field observations. *Journal of Geophysical Research,* 112, C03001, doi: 10.1029/2005JC002893.
Mariño-Tapia, I.; O'Hare, T.; Russell, P.; Davidson, M., and Huntley, D., 2007b. Cross-shore sediment transport on natural beaches and their relation to sand bar migration patterns, part 2: applications of the field transport parameterization. *Journal of Geophysical Research,* 112, C03002, doi: 10.1029/2005JC002894.
Masselink, G., 2004. Formation and evolution of multiple intertidal bars on macrotidal beaches: application of a morphodynamic model. *Coastal Engineering,* 51, 713–730.
Masselink, G.; Evans, D.; Hughes, M., and Russell, P., 2005. Suspended sediment transport in the swash zone of a dissipative beach. *Marine Geology,* 216, 169–189.
Masselink, G. and Hughes, M. 1998. Field investigation of sediment transport in the swash-zone. *Continental Shelf Research,* 18, 1179–1199.
Masselink, G. and Puleo, J., 2006. Swash-zone morphodynamics. *Continental Shelf Research,* 26, 661–680.
Masselink, G. and Russell, P., 2006. Flow velocities, sediment transport and morphological change in the swash zone of a dissipative and reflective beach. *Marine Geology,* 227, 227–240.
Masselink, G. and Short, A., 1993. The effect of tide range on beach morphodynamics and morphology—a conceptual beach model. *Journal of Coastal Research,* 9, 785–800.
McCowen, J., 1894. On the highest wave of permanent type. *Philosophical Magazine,* Series 5, 38, 351–357.
Miles, J.; Butt, T., and Russell, P., 2006. Swash zone sediment dynamics: a comparison of a dissipative and an intermediate beach. *Marine Geology,* 231, 181–200.
Miller, H. C., 1999. Field measurements of longshore sediment transport during storms. *Coastal Engineering,* 36, 301–321.
Nielsen, P., 1998. Coastal groundwater dynamics. *In: Proceedings of Coastal Dynamics '97.* (Plymouth, U.K., ASCE), pp. 546–555.
Nielsen, P., 2002. Shear stress and sediment transport calculations for swash zone modelling. *Coastal Engineering,* 45, 53–60.
Nielsen, P., 2006. Sheet flow sediment transport under waves with acceleration skewness and boundary layer streaming. *Coastal Engineering,* 53, 749–758.
Osborne, P. and Rooker, G., 1999. Sand re-suspension events in a high-energy infragravity swash zone. *Journal of Coastal Research,* 15, 74–86.
Petti, M. and Longo, S., 2001. Turbulence experiments in the swash zone. *Coastal Engineering,* 43, 1–24.
Plant, N.; Ruessink, B.G., and Wijnberg, K., 2001. Morphologic properties derived from a simple cross-shore sediment transport model. *Journal of Geophysical Research,* 106, 945–958.
Plant, N.; Holland, K.T.; Puleo, J., and Gallagher, E., 2004. Prediction skill of nearshore profile evolution models. *Journal of Geophysical Research,* 109, C01006, doi: 10.1029/2003JC001995.
Pritchard, D. and Hogg, A., 2005. On the transport of suspended sediment by a swash event on a plane beach. *Coastal Engineering,* 52, 1–23.
Puleo, J.; Beach, R.; Holman, R., and Allen, J., 2000. Swash zone sediment suspension and transport and the importance of bore-generated turbulence. *Journal of Geophysical Research,* 105, 17021, doi: 10.1029/2000JC900024.
Puleo, J.; Holland, K.; Plant, N.; Slinn, D., and Hanes, D., 2003. Fluid acceleration effects on suspended sediment transport in the swash zone. *Journal of Geophysical Research,* 108, 3350, doi: 10.1029/2003JC001943.
Russell, P. and Huntley, D.A., 1999. A cross-shore transport "shape function" for high energy beaches. *Journal of Coastal Research,* 15, 198–205.
Tinker, J.; Russell, P.; Masselink, G.; O'Hare, T.; Butt, T.; Austin, M.; Ganderton, P., and Gallagher, E., 2006 Field measurements of velocity moment shape functions (The X-SHORE Project). *In: Proceedings of 30th International Conference on Coastal Engineering,* San Diego: World Scientific, pp. 3987–3999.
Turner, I. and Masselink, G., 1998. Swash infiltration-exfiltration and sediment transport. *Journal of Geophysical Research,* 103, 30813–30824.
Weir, F.; Hughes, M., and Baldock, T., 2006. Beach face and berm morphodynamics facing a frontal lagoon. *Geomorphology,* 82, 331–346.